JACS
JOURNAL OF THE AMERICAN CHEMICAL SOCIETY

Article

pubs.acs.org/JACS

Highly Accurate Excited-State Structure of $[Os(bpy)_2dcbpy]^{2+}$ Determined by X-ray Transient Absorption Spectroscopy

Xiaoyi Zhang,*[,†] Sophie E. Canton,[‡] Grigory Smolentsev,[§] Carl-Johan Wallentin,[∥] Yizhu Liu,[∥] Qingyu Kong,[†] Klaus Attenkofer,[†,○] Andrew. B. Stickrath,[#,◆] Michael W. Mara,[⊥] Lin X. Chen,[⊥,#] Kenneth Wärnmark,[∥] and Villy Sundström[▽]

[†]X-ray Sciences Division, Argonne National Laboratory, Argonne, Illinois 60439, United States
[‡]Department of Synchrotron Radiation Instrumentation, Lund University, P.O. Box 118, 22100 Lund, Sweden
[§]Paul Scherrer Institut, WLGA 217, 5232 Villigen, Switzerland
[∥]Centre for Analysis and Synthesis, Department of Chemistry, Lund University, 22100 Lund, Sweden
[⊥]Department of Chemistry, Northwestern University, Evanston, Illinois 60208, United States
[#]Chemical Sciences and Engineering Division, Argonne National Laboratory, Argonne, Illinois 60439, United States
[▽]Department of Chemical Physics, Lund University, P.O. Box 124, 22100 Lund, Sweden

Supporting Information

ABSTRACT: Determining the electronic and geometric structures of photoexcited transient species with high accuracy is crucial for understanding their fundamental photochemistry and controlling their photoreactivity. We have applied X-ray transient absorption spectroscopy to measure the XANES and EXAFS spectra of a dilute (submillimolar) solution of the osmium(II) polypyridyl complex $[Os(bpy)_2dcbpy](PF_6)_2$ (dcbpy = 4,4′-dicarboxy-2,2′-bipyridine) (OsL_2L') in methanol at the Os L_{III} edge. We have obtained spectra of superb quality for both the ground state and the photoinduced ^{3}MLCT excited state that have allowed us not only to extract detailed information about the Os 5d orbitals but also to resolve very small differences of 0.010 ± 0.008 Å in the average Os−N bond lengths of the ground and excited states. Theoretical calculations using a recently developed DFT-based approach support the measured electronic structures and further identify the nature of the molecular orbitals that contribute to the main absorption bands in the XANES spectra.

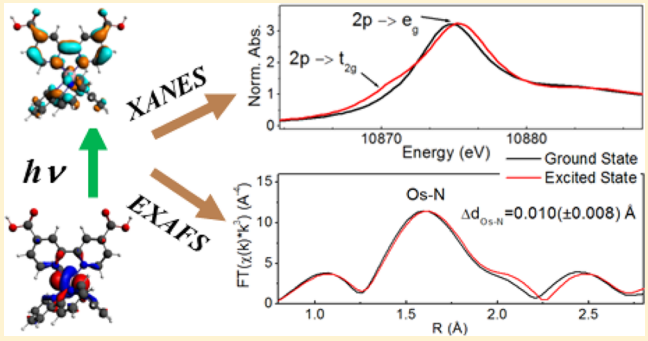

INTRODUCTION

The metal-to-ligand charge transfer (MLCT) excited states of ruthenium and osmium polypyridyl complexes and their derivatives have superior photophysical and photochemical properties, such as intense absorption bands that match a large fraction of the solar spectrum, long excited-state lifetimes, strong luminescence, and highly efficient electron injection to the conduction band of semiconductor nanocrystals.[1−3] Therefore, the MLCT states of Ru and Os transition-metal compounds have versatile applications in solar energy utilization and other fields ranging from molecular electronics and photocatalysis to light-emitting devices and biolabels.[1−8]

The MLCT excitation induced by light absorption corresponds to an electron transfer from metal-centered molecular orbitals (MOs) with d character to ligand-centered (LC) MOs with π^* character. Because the electronic and geometrical structures of molecular systems are strongly correlated with their functionalities and often govern the outcomes of photoinduced reactions, in-depth structural information on MLCT states is important for the rational design of solar energy devices. Over the past several decades, the MLCT states of Ru compounds have been intensely studied using a wealth of techniques.[1−4,6,9,10] The recent development of X-ray transient absorption (XTA) spectroscopy has made it possible to directly probe the transient electronic and molecular structures of photoexcited species.[9,11−18] Studies of the transient structure of photoexcited $[Ru^{II}(bpy)_3]^{2+}$ (bpy = 2,2′-bipyridine) showed a shrinkage of about 0.03−0.04 Å in the average Ru−N bond distance in the MLCT state compared with the ground state.[9,18,19] Later on, the same technique was applied to capture the structural changes of $Ru(dcbpy)_2(NCS)_2$ (dcbpy = 4,4′-dicarboxy-2,2′-bipyridine) dye molecules adsorbed onto a TiO_2 nanoparticle surface accompanying photoinduced electron injection from the dye to TiO_2.[15] The average Ru−N_{NCS} bond length shortens by about 0.06 Å in going from the ground state to the transient charge-separated

Received: April 23, 2014
Published: May 29, 2014

 © 2014 American Chemical Society

state, while the average Ru−N_{dcbpy} bond length remains unchanged.

Compared with their Ru analogues, Os compounds present extra absorption at longer wavelengths that enhances the solar photon absorption efficiency. Figure 1 shows the UV−vis

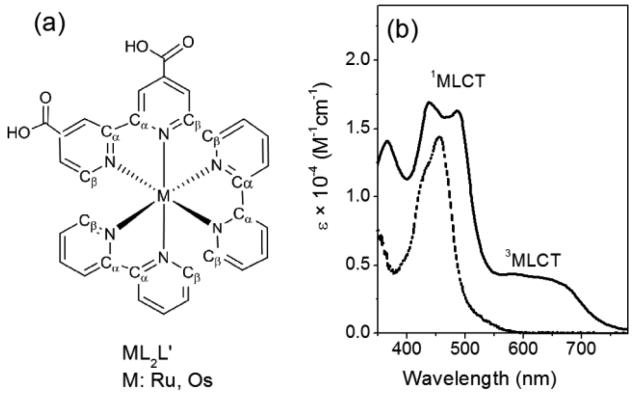

Figure 1. (a) Chemical structure of Os(Ru)L_2L'. (b) UV−vis absorption spectra of OsL_2L' (solid line) and RuL_2L' (dashed line) in methanol.

absorption spectra of $[Os(bpy)_2dcbpy](PF_6)_2$ and $[Ru(bpy)_2dcbpy](PF_6)_2$ (abbreviated as OsL_2L' and RuL_2L', respectively). The intense absorption between 400 and 550 nm is ascribed to the transition from the $^1A_1$ ground state to the ^{1}MLCT state. Another broad absorption band at longer wavelength (550−750 nm) can be observed in the spectrum of OsL_2L'. This band originates from photoexcitation directly to the ^{3}MLCT state. The ^{3}MLCT transition becomes allowed as a result of the strong spin−orbit coupling induced by the 5d electrons, while it is much weaker in the Ru analogues. Studies of a series of Os polypyridyl dyes attached to TiO_2 nanoparticles have shown that they can achieve photoelectrochemical performance similar to that of the efficient Ru dyes.[5,7,20]

Despite these clear advantages, much fewer studies have been done on Os polypyridyl complexes for solar energy applications. In particular, knowledge about the transient electronic and geometric structures of their photoexcited form is extremely limited from both the experimental and theoretical points of view. The theoretical calculations are fairly intensive because of the relativistic effects induced by the heavy Os atom; the influence of spin−orbit coupling cannot be ignored. In this work, we have applied XTA spectroscopy at the L_{III} edge and density functional theory (DFT) to study the transient ^{3}MLCT excited state of OsL_2L'. We have obtained XTA spectra with unprecedented signal-to-noise ratio that have allowed us to determine the internuclear distances of OsL_2L' with less than 0.01 Å uncertainty for both the ground and excited states. The information obtained from this study, such as ligand-field splitting strength, orbital energy levels, and local geometric structure, are of fundamental importance not only for Os complexes in dye-sensitized solar cells (DSSCs) but also for general molecular designs in solar energy applications.

EXPERIMENTAL SECTION

$[Os(bpy)_2dcbpy](PF_6)_2$ ($Os^{II}L_2L'$),[5] $[Os^{II}(bpy)_3](PF_6)_2$ ($Os^{II}L_3$),[21] and $[Os^{III}(bpy)_3](PF_6)_3$ ($Os^{III}L_3$)[22] were prepared using literature procedures. All of the other chemicals were purchased from Aldrich and used as received.

The XTA measurements used laser "pump" pulses to initiate the MLCT transition of OsL_2L' and X-ray "probe" pulses at a certain delay time with respect to the pump pulses to monitor the transient structural changes by X-ray absorption spectroscopy.The XTA measurements were carried out on beamline 11-ID-D of the Advanced Photon Source (APS) at Argonne National Laboratory. The 527 nm, 5 ps full width at half-maximum (fwhm), 1.6 kHz laser pulses given by the second-harmonic output of a Nd:YFL regenerative amplified laser were used as the pump pulses. The X-ray pulses were the single-electron bunch extracted from the storage ring at 271.6 kHz operated under the hybrid timing mode. The time resolution of the XTA measurements was 160 ps as determined by the fwhm of the X-ray pulses provided by the APS. A detailed experimental description is given in the Supporting Information (SI).

RESULTS AND DISCUSSION

(1). XANES Spectra by XTA Spectroscopy. Figure 2a shows the Os L_{III}-edge X-ray absorption near-edge fine

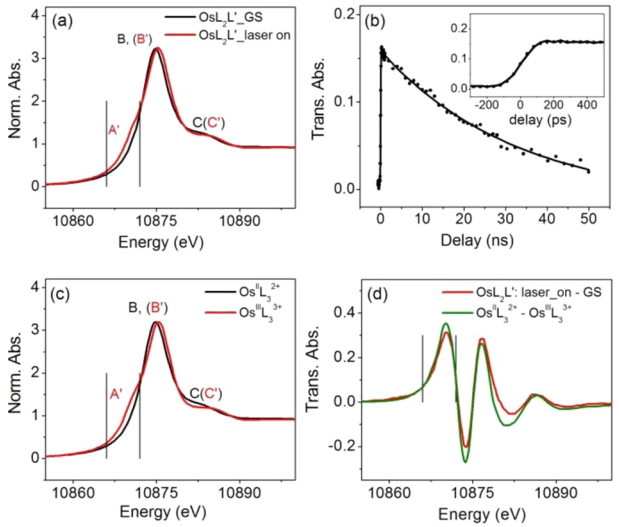

Figure 2. (a) XANES spectra of a 0.8 mM solution of $Os^{II}L_2L'$ in methanol measured at the Os L_{III} edge. The black curve is the ground-state spectrum, and the red curve is the spectrum measured 400 ps after laser excitation. (b) X-ray transient absorption kinetics probed at the 2p → t_{2g} transition peak (10870.7 eV) at delay times from −0.6 to 50 ns. The inset shows the rise of the transient absorption at early delay times. (c) Ground-state XANES spectra of 0.8 mM solutions of $Os^{II}L_3$ (black) and $Os^{III}L_3$ (red) in acetonitrile. (d) The difference XANES spectrum between laser-on (400 ps delay) and laser-off for $Os^{II}L_2L'$ (red) and the difference XANES spectrum between $Os^{II}L_3$ and $Os^{III}L_3$ (green).

structure (XANES) spectra of OsL_2L' in methanol with and without laser excitation. The laser-on spectrum was recorded at a 400 ps delay after the laser pump pulse. The intense absorption band corresponds to the dipole-allowed transition from the $2p_{3/2}$ level to the unoccupied 5d orbitals. Therefore, the L_{III}-edge XANES spectra directly measure the occupancy of the metal d orbitals. On the basis of ligand-field theory, the five 5d orbitals of Os split into doubly degenerate e_g orbitals and triply degenerate t_{2g} orbitals in an ideal octahedral coordination environment. In the $^1A_1$ ground state, the six 5d electrons occupy the three t_{2g} orbitals. The so-called white line (B band) in the ground-state spectrum is attributed to the transition from the $2p_{3/2}$ level to the empty e_g orbitals. The laser-on spectrum shows an additional absorption band (A′) on the low-energy side of the main band (B′) that indicates an extra 2p → 5d

dx.doi.org/10.1021/ja5040733 | J. Am. Chem. Soc. 2014, 136, 8804−8809

transition in the excited state. The 527 nm laser excites the OsL_2L' to the ^{1}MLCT state. According to previous time-resolved laser spectroscopy studies, this photoexcited state relaxes to the lowest ^{3}MLCT state on the subpicosecond to tens of picoseconds time scale.[23,24] In the ^{3}MLCT state, one electron has been transferred from the t_{2g} orbital to a nearby ligand, leaving a half-filled t_{2g} orbital. Consequently, the A′ band in the spectrum of the ^{3}MLCT state corresponds to the $2p \rightarrow t_{2g}$ transition.

Figure 2b shows the X-ray transient absorption kinetics measured at the maximum of the $2p \rightarrow t_{2g}$ transition of the ^{3}MLCT state (10870.7 eV). The inset shows the rise of the difference absorption around time zero, which corresponds to the appearance of the ^{3}MLCT state. On the basis of these X-ray transient kinetic measurements, the rise of the transient signal takes about 160 ps, which is limited by the duration of the X-ray probe pulses. The photoexcited species measured at a 400 ps delay should be mainly in the ^{3}MLCT state. The kinetic trace was fitted with a single-exponential decay convoluted with a Gaussian function of 160 ps fwhm representing the X-ray pulse width. The lifetime of the ^{3}MLCT state obtained from the fitting of the kinetic trace is 33 ± 2 ns.

In order to obtain the pure spectrum of the ^{3}MLCT excited state, one must know the excited-state fraction at a delay of 400 ps after the laser excitation probed by the X-ray pulses. One significant change after laser excitation is that the Os oxidation state has increased from +2 to +3, resulting in an extra $2p \rightarrow t_{2g}$ transition in the excited state. We measured the static XANES spectra of the two reference compounds $[Os^{II}(bpy)_3](PF_6)_2$ ($Os^{II}L_3$) and $[Os^{III}(bpy)_3](PF_6)_3$ ($Os^{III}L_3$) in order to get the XANES spectra of 100% Os^{II} and 100% Os^{III} (Figure 2c). Figure 2d displays the difference XANES spectrum with and without laser excitation for $Os^{II}L_2L'$ (red) and the difference XANES spectrum between $Os^{II}L_3$ and $Os^{III}L_3$ (green). The positive difference absorption between 10866 and 10719 eV corresponds to the $2p \rightarrow t_{2g}$ transition in Os^{III}. By comparison of the integrated areas between 10866 and 10719 eV for the two different XANES features in Figure 2d, the excited-state fraction for the laser-on spectra was determined to be 0.89. Such a high excited-state population is attributable to the combination of a dilute sample (0.8 mM), a high absorption coefficient, and a high photon density per pulse.

The Os L_{III}-edge XANES spectra of the ground state and ^{3}MLCT excited state were fitted with a sum of an arctangent function for the edge-jump absorption and several pseudo-Voigt functions to represent the absorption bands (Figure 3). The peak positions extracted from the fitting are listed in Table 1S in the SI. The 4.6 eV energy difference between A′ and B′ directly measures the ligand-field spitting between the e_g and t_{2g} orbitals (denoted as Δ) in the ^{3}MLCT state. The $2p \rightarrow e_g$ orbital transition energy is blue-shifted by 0.5 eV from 10874.8 to 10875.3 eV in changing from the $^1A_1$ state to the ^{3}MLCT state. Furthermore, there is a shoulder [labeled as C (C′)] in the higher-energy tail of the B (B′) band that originates from transitions from the 2p to other empty molecular orbitals below the ionization potential.

(2). EXAFS Spectra by XTA Spectroscopy. Figure 4a,b shows the extended X-ray absorption fine structure (EXAFS) spectra of 0.8 mM OsL_2L' in methanol in *k* space and the magnitude of the phase-uncorrected Fourier transformed EXAFS spectra in *R* space. There is no significant difference between the EXAFS spectra of the $^1A_1$ and the ^{3}MLCT states. Consequently, only small structural changes upon laser

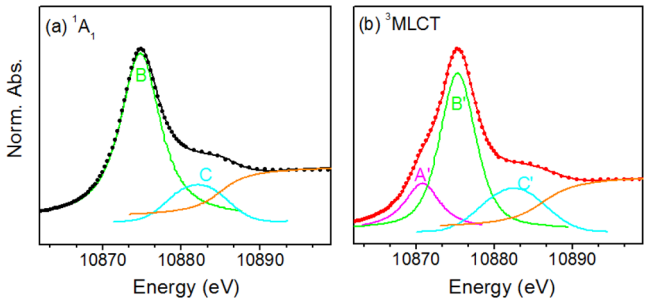

Figure 3. Os L_{III}-edge XANES spectra (solid circles) of OsL_2L' in methanol in (a) the ground state ($^1A_1$) and (b) the ^{3}MLCT state. The solid lines are the respective fitted curves as described in the text. The contributions of the individual absorption bands and the edge jump obtained from the fitting are also displayed.

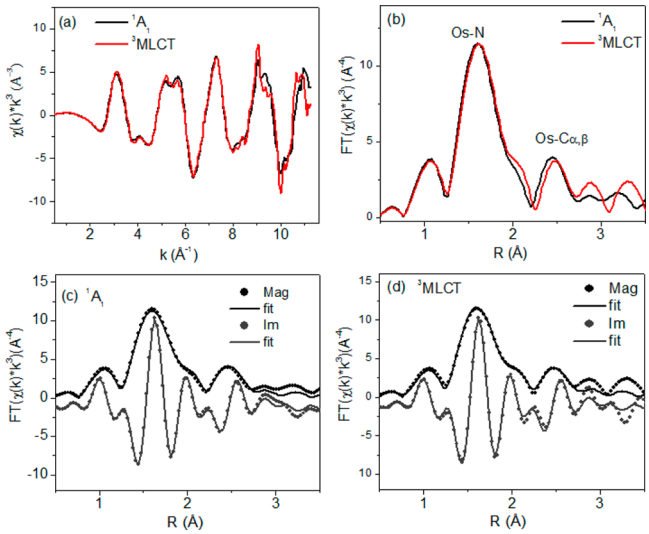

Figure 4. (a, b) Os L_{III}-edge EXAFS spectra of 0.8 mM OsL_2L' in methanol for both the $^1A_1$ state and the ^{3}MLCT state in (a) *k* space and (b) *R* space. A *k*-space range of 2.4 to 11.2 Å^{-1} was used for the Fourier transform to *R* space. (c, d) Fourier transformed EXAFS spectra of OsL_2L' and best fits for (c) the $^1A_1$ state and (d) the ^{3}MLCT state. The spectra are phase-uncorrected, so the distances *R* shown in the figure are smaller than the actual values.

excitation are expected. The peaks between 1 and 2 Å are associated with the Os−N bond distance, and they are slightly shifted to higher positions in the excited state (Figure 4b). The k^3-weighted Fourier transformed EXAFS spectra with *k* ranging from 2.4 to 11.2 Å^{-1} are fitted in *R* space in the range of 1−3.2 Å. The contributions from all of the paths in the first two scattering shells (Os−N and Os−$C_{\alpha,\beta}$) were included in the fitting. The atoms involved in those paths are labeled in Figure 1a. The magnitudes and imaginary parts of the *R*-space fittings of the Fourier transformed EXAFS spectra for the $^1A_1$ and ^{3}MLCT states are displayed in Figure 4c,d, respectively.

Table 1 lists the main structural parameters of the Os−N and Os−$C_{\alpha,\beta}$ shells for both the $^1A_1$ and the ^{3}MLCT states as extracted from the EXAFS data analysis. Detailed analysis can be found in the SI. These high-quality XTA spectra allow us to determine the bond lengths in the ground and excited states with picometer resolution. The average distances between Os and the first-shell nitrogens are 2.066 ± 0.005 Å for the $^1A_1$ state and 2.076 ± 0.006 for the ^{3}MLCT state. The bond-length change is small, and the direction of the change is opposite to

dx.doi.org/10.1021/ja5040733 | J. Am. Chem. Soc. 2014, 136, 8804−8809

Table 1. Electronic and Structural Parameters of OsL_2L' Determined by XTA Measurements and DFT Calculations

		$^1A_1$ (E_0 = 10884.9 ± 1.1 eV; S_0^2 = 0.90 ± 0.08)			^{3}MLCT (E_0 = 10886.2 ± 1.2 eV; S_0^2 = 0.80 ± 0.11)				
method	bond	N	R (Å)	σ^2 (Å^2)	N	R (Å)	σ^2 (Å^2)	$\Delta E_{B'-A'}$ (eV)	$\Delta E_{B'-B}$ (eV)
XTA	Os−N	6	2.066 ± 0.005	0.0008 ± 0.0007	6	2.076 ± 0.006	0.0004 ± 0.0007	4.6 ± 0.1	0.6 ± 0.1
	Os−C_α	6	2.940 ± 0.014	0.004 ± 0.002	6	2.947 ± 0.017	0.004 ± 0.002		
	Os−C_β	6	3.052 ± 0.014	0.004 ± 0.002	6	3.058 ± 0.017	0.004 ± 0.002		
DFT	Os−N	6	2.03		6	2.03		5.0	0.7

that of RuL_3^{2+}, which shows a 0.03−0.04 Å decrease in the ^{3}MLCT state.[9,18] The bonding between Ru/Os and N_{bpy} contains two components: the donation of the lone-pair electron density from nitrogen to an empty metal d orbital through σ bonding and electron density donation from a metal d orbital to a ligand π^* orbital through π back-bonding. Upon photoexcitation, the metal center of the Ru/Os polypyridyl complex loses electron density, which causes two competing effects on the Ru/Os−N bond order: (1) strengthening of the Ru/Os−N σ bonding and (2) weakening of the π back-bonding. In RuL_3, the first effect is stronger than the second one, so the Ru−N bond length is decreased by ∼0.03−0.04 Å in the ^{3}MLCT state. In Os compounds, the stronger spin−orbit coupling further splits the three t_{2g} orbitals, which brings one of them closer to the ligand π^* orbital. Johansson et al.[25] investigated the electronic structure of a series of ML_3^{2+} complexes (M = Fe, Ru, Os) using photoelectron spectroscopy and observed that one of the t_{2g} orbitals in OsL_3^{2+} is about 0.6 eV closer to the ligand π^* orbital than that of RuL_3^{2+}. The smaller energy difference between the occupied metal-centered t_{2g} orbital and the ligand π^* orbital of the Os complex increases the π back-bonding effect in comparison with its Ru analogue. Therefore, in OsL_2L' the weakening of the π back-bonding in the conversion from the $^1A_1$ to the ^{3}MLCT state overwhelms the strengthening of the σ bonding, resulting in an Os−N bond length elongation of 0.010 ± 0.008 Å. The present results are very similar to the Os−N bond lengths obtained from X-ray diffraction (XRD) measurements, which are 2.061 ± 0.008 Å for $Os^{II}L_3$ and 0.01 Å longer for $Os^{III}L_3$ in general.[26] A very recent time-dependent DFT calculation on $Os^{II}L_3$ gave an average Os−N bond length of 2.074 Å,[27] which is only 0.008 Å longer than the Os−N bond length obtained in our measurements on OsL_2L' in the $^1A_1$ ground state.

(3). DFT-Based Calculations. In order to gain further understanding of the electronic excited state and visualize the molecular orbitals that contribute to the XANES spectral features, we calculated the Os L_{III}-edge XANES spectra of the $^1A_1$ and ^{3}MLCT states using approaches based on the two-component relativistic zeroth-order regular approximation (ZORA) implemented in DFT.[28] These calculations also take into consideration the spin−orbit coupling and the hybridization between the Os 5d and ligand orbitals. Unlike calculations using the FEFF and FDMNES programs, this approach does not require the input of the Fermi energy, which is not so easy to define a priori, implying that the shapes of the XANES spectra given by this approach are generally more reliable.[28]

On the basis of the calculations, the highest occupied molecular orbital (HOMO) of the $^1A_1$ state has electron density localized around Os, while the lowest unoccupied molecular orbital (LUMO) has electron density residing on the ligands (Figure 5a). Figure 5b shows the calculated Os L_{III}-edge XANES spectra for both the $^1A_1$ and the ^{3}MLCT states. The

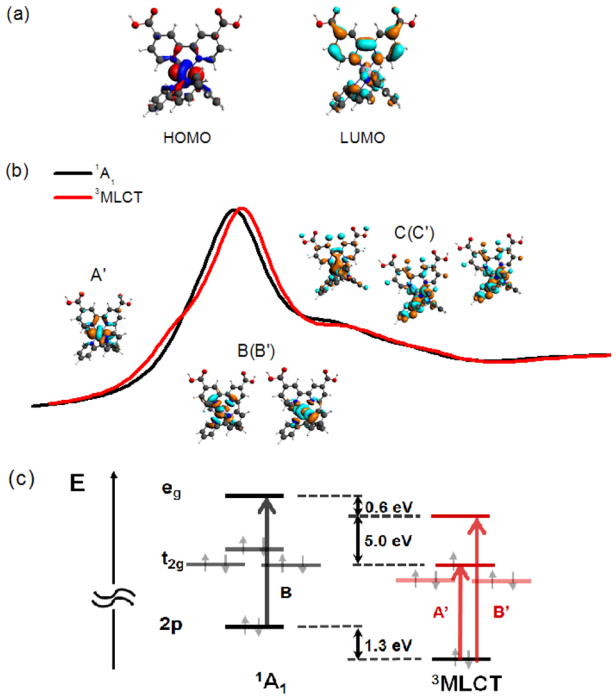

Figure 5. (a) Electronic structures of the HOMO and LUMO of OsL_2L' in the $^1A_1$ state from the calculations. (b) Calculated XANES spectra of both the $^1A_1$ state and the ^{3}MLCT state. The electronic structures of the molecular orbitals contributing to the main transition bands in the XANES spectra are also displayed. (c) Energy levels of the molecular orbitals involved in 2p → 5d transitions obtained from the calculations.

calculated spectra agree well with the experimental data. The molecular orbital that contributes to the A′ feature is very similar to the HOMO orbital of the $^1A_1$ state. Photoexcitation induces electron transfer from the HOMO to the LUMO, leaving an Os 5d orbital vacancy in the HOMO. The HOMO of the $^1A_1$ state becomes the LUMO of the ^{3}MLCT state, and the transition from 2p to this LUMO gives rise to the A′ feature in the XANES spectrum of the ^{3}MLCT state. As can be seen from Figure 5b, the molecular orbitals contributing to the A′ and B (B′) transitions have mainly Os 5d orbital character as expected, while those contributing to C (C′) have substantial contributions from both metal d orbitals and ligand orbitals, which indicates that the C (C′) band originates from hybridization of the Os 5d and ligand orbitals.

The calculations also provide quantitative information about the geometric structures and the molecular orbital energies. Table 1 compares the main electronic and structural parameters extracted from the experiments and calculations. The average Os−N bond length from the calculations is 2.03 Å for both states, which is 0.03−0.04 Å shorter than those extracted from the TXA measurements. The energy difference between the A′

dx.doi.org/10.1021/ja5040733 | J. Am. Chem. Soc. 2014, 136, 8804−8809

and B′ bands ($\Delta E_{B'-A'}$) of OsL_2L' in the ^{3}MLCT state characterizes the ligand-field splitting (Δ). $\Delta E_{B'-A'}$ of OsL_2L' from the calculations is 5.0 eV, which is close to the experimentally measured value of 4.6 eV. The calculation indicates a 0.7 eV increase in the energy of the 2p → e_g transition of the ^{3}MLCT state in comparison with the $^1A_1$ state. The XTA measurement gave a similar increase of 0.5 eV. However, the calculations reveal the absolute energy changes of molecular orbitals in going from the $^1A_1$ state to the ^{3}MLCT state, which cannot be obtained directly from the XTA measurements. The 2p core orbital and the e_g orbital are lowered by 1.3 and 0.6 eV, respectively, during the transition from the $^1A_1$ state to the ^{3}MLCT state (Figure 5c). The reduced electron density at the Os center in the ^{3}MLCT excited state increases the screening effect and therefore stabilizes the molecular orbitals.

SUMMARY

We have obtained accurate electronic and geometric structural information for the Os^{II} polypyridyl complex $[Os(bpy)_2dcbpy](PF_6)_2$ in methanol in both the ground state and the ^{3}MLCT photoexcited state using XTA spectroscopy. We have achieved spatial resolution of less than 0.01 Å, allowing us to resolve an average Os−N bond distance change of (0.010 ± 0.008) Å in the excited state. Information regarding the molecular orbital energies, such as the ligand field splitting and absorption band positions, also agree with our DFT-based calculations. The calculations give further insight into the origin of the transitions and reveal how the electron density changes affect the orbital energy levels.

The ability to determine ground-state and transient structures with high accuracy provides new insights into fundamental photochemistry. With the quality of XTA spectra now reaching that of static X-ray absorption spectra, XTA spectroscopy can be used on not only the relatively simple model systems for which extensive photochemical and photophysical knowledge exist but also on general solar energy conversion processes with complex changes of electronic and atomic structures. XTA measurements combined with calculations can provide crucial information for realizing the rational design of molecular systems for efficient solar energy applications.

ASSOCIATED CONTENT

Supporting Information

Additional details concerning XTA measurements, XANES and EXAFS data analysis, and DFT-based calculations. This material is available free of charge via the Internet at http://pubs.acs.org.

AUTHOR INFORMATION

Corresponding Author

xyzhang@aps.anl.gov

Present Addresses

○K.A.: Brookhaven National Laboratory, Upton, NY 11973, USA.

◆A.B.S.: Booz Allen Hamilton, 3811 North Fairfax Drive, Suite 600, Arlington, VA 22203, USA.

Notes

The authors declare no competing financial interest.

ACKNOWLEDGMENTS

This work was supported by the U.S. Department of Energy, Office of Science, Office of Basic Energy Sciences, under Contract DE-AC02-06CH11357. S.E.C. acknowledges support from the Swedish Research Council. V.S. was supported by the Swedish Research Council and the European Research Council via Contract ERC-AdvG-VISCHEM-226136. G.S. was supported by the Swiss National Science Foundation (Grant 200021-135226) and the European Commission's Seventh Framework Program (FP7/2007-2013) under Grant Agreement 290605 (COFUND: PSI-FELLOW). Use of the Advanced Photon Source at Argonne National Laboratory was supported by the U.S. Department of Energy, Office of Science, Office of Basic Energy Sciences, under Contract DE-AC02-06CH11357.

REFERENCES

(1) Ardo, S.; Meyer, G. J. *Chem. Soc. Rev.* **2009**, *38*, 115.
(2) Campagna, S.; Puntoriero, F.; Nastasi, F.; Bergamini, G.; Balzani, V. *Top. Curr. Chem.* **2007**, *280*, 117.
(3) Hagfeldt, A.; Grätzel, M. *Acc. Chem. Res.* **2000**, *33*, 269.
(4) Oregan, B.; Grätzel, M. *Nature* **1991**, *353*, 737.
(5) Sauve, G.; Cass, M. E.; Coia, G.; Doig, S. J.; Lauermann, I.; Pomykal, K. E.; Lewis, N. S. *J. Phys. Chem. B* **2000**, *104*, 6821.
(6) Vrábel, M.; Horáková, P.; Pivoňková, H.; Kalachova, L.; Černocká, H.; Cahová, H.; Pohl, R.; Šebest, P.; Havran, L.; Hocek, M.; Fojta, M. *Chem.—Eur. J.* **2009**, *15*, 1144.
(7) Wu, K.-L.; Ho, S.-T.; Chou, C.-C.; Chang, Y.-C.; Pan, H.-A.; Chi, Y.; Chou, P.-T. *Angew. Chem., Int. Ed.* **2012**, *51*, 5642.
(8) Zhao, Q.; Li, F.; Huang, C. *Chem. Soc. Rev.* **2010**, *39*, 3007.
(9) Saes, M.; Bressler, C.; Abela, R.; Grolimund, D.; Johnson, S. L.; Heimann, P. A.; Chergui, M. *Phys. Rev. Lett.* **2003**, *90*, No. 047403.
(10) Anderson, N. A.; Lian, T. Q. *Annu. Rev. Phys. Chem.* **2005**, *56*, 491.
(11) Bressler, C.; Milne, C.; Pham, V. T.; ElNahhas, A.; van der Veen, R. M.; Gawelda, W.; Johnson, S.; Beaud, P.; Grolimund, D.; Kaiser, M.; Borca, C. N.; Ingold, G.; Abela, R.; Chergui, M. *Science* **2009**, *323*, 489.
(12) Chen, L. X.; Zhang, X. *J. Phys. Chem. Lett.* **2013**, *4*, 4000.
(13) Lima, F. A.; Milne, C. J.; Amarasinghe, D. C.; Rittmann-Frank, M. H.; van der Veen, R. M.; Reinhard, M.; Pham, V. T.; Karlsson, S.; Johnson, S. L.; Grolimund, D.; Borca, C.; Huthwelker, T.; Janousch, M.; van Mourik, F.; Abela, R.; Chergui, M. *Rev. Sci. Instrum.* **2011**, *82*, No. 063111.
(14) March, A. M.; Stickrath, A.; Doumy, G.; Kanter, E. P.; Krässig, B.; Southworth, S. H.; Attenkofer, K.; Kurtz, C. A.; Chen, L. X.; Young, L. *Rev. Sci. Instrum.* **2011**, *82*, No. 073110.
(15) Zhang, X. Y.; Smolentsev, G.; Guo, J. C.; Attenkofer, K.; Kurtz, C.; Jennings, G.; Lockard, J. V.; Stickrath, A. B.; Chen, L. X. *J. Phys. Chem. Lett.* **2011**, *2*, 628.
(16) Van Kuiken, B. E.; Huse, N.; Cho, H.; Strader, M. L.; Lynch, M. S.; Schoenlein, R. W.; Khalil, M. *J. Phys. Chem. Lett.* **2012**, *3*, 1695.
(17) Katz, J. E.; Zhang, X. Y.; Attenkofer, K.; Chapman, K. W.; Frandsen, C.; Zarzycki, P.; Rosso, K. M.; Falcone, R. W.; Waychunas, G. A.; Gilbert, B. *Science* **2012**, *337*, 1200.
(18) Sato, T.; Nozawa, S.; Tomita, A.; Hoshino, M.; Koshihara, S.-y.; Fujii, H.; Adachi, S.-i. *J. Phys. Chem. C* **2012**, *116*, 14232.
(19) Gawelda, W.; Johnson, M.; de Groot, F. M. F.; Abela, R.; Bressler, C.; Chergui, M. *J. Am. Chem. Soc.* **2006**, *128*, 5001.
(20) Kinoshita, T.; Fujisawa, J.-i.; Nakazaki, J.; Uchida, S.; Kubo, T.; Segawa, H. *J. Phys. Chem. Lett.* **2012**, *3*, 394.
(21) Nakabayashi, Y.; Nakamura, K.; Kawachi, M.; Motoyama, T.; Yamauchi, O. *J. Biol. Inorg. Chem.* **2003**, *8*, 45.
(22) Gagliardi, C. J.; Binstead, R. A.; Thorp, H. H.; Meyer, T. J. *J. Am. Chem. Soc.* **2011**, *133*, 19594.
(23) Shaw, G. B.; Brown, C. L.; Papanikolas, J. M. *J. Phys. Chem. A* **2002**, *106*, 1483.

(24) Shaw, G. B.; Styers-Barnett, D. J.; Gannon, E. Z.; Granger, J. C.; Papanikolas, J. M. *J. Phys. Chem. A* **2004**, *108*, 4998.
(25) Johansson, E. M. J.; Odelius, M.; Plogmaker, S.; Gorgoi, M.; Svensson, S.; Siegbahn, H.; Rensmo, H. *J. Phys. Chem. C* **2010**, *114*, 10314.
(26) Demadis, K. D.; Dattelbaum, D. M.; Kober, E. M.; Concepcion, J. J.; Paul, J. J.; Meyer, T. J.; White, P. S. *Inorg. Chim. Acta* **2007**, *360*, 1143.
(27) Ronca, E.; De Angelis, F.; Fantacci, S. *J. Phys. Chem. C* **2014**, DOI: 10.1021/jp500869r.
(28) Alperovich, I.; Smolentsev, G.; Moonshiram, D.; Jurss, J. W.; Concepcion, J. J.; Meyer, T. J.; Soldatov, A.; Pushkar, Y. *J. Am. Chem. Soc.* **2011**, *133*, 15786.